scientific reports

Check for updates

OPEN

Ratiometric fluorescence nanoprobe based on nitrogen-doped carbon dots for Cu^{2+} and Fe^{3+} detection

Chunlei Yang✉, Guiju Xu, Chenghao Hou & Hongwei Zhang✉

Heavy metal ions pollution in environmental waters has an increasing impact on human health. As two common metal ions, copper ions (Cu^{2+}) and ferric ions (Fe^{3+}) widely exist in nature and play a vital role in life process. Therefore, it is significant to design sensitive and simple detection approaches for Cu^{2+} and Fe^{3+}. In our work, the ratiometric fluorescence analysis method (denoted as N-CDs/OPD) was established for Cu^{2+} and Fe^{3+} detection. The N-CDs exhibited a Cu^{2+} and Fe^{3+} fluorescence quenching response properties. The o-phenylenediamine (OPD) may be oxidized to 2,3-diaminophenazine (DAP) by Cu^{2+} and Fe^{3+}. With addition of Cu^{2+} or Fe^{3+}, the fluorescence of N-CDs (436 nm) was quenched and a new peak at 556 nm (DAP) appeared, which realized fluorescent ratiometric detection of Cu^{2+} and Fe^{3+}. The Cu^{2+} concentration shows a good linear correlation versus fluorescence ratio (F_{436}/F_{556}) in the range of 10 to 30 μM ($R^2 = 0.9981$) with detection limit (LOD) of 0.86 μM. In addition, a good linear relationship between fluorescence ratio (F_{436}/F_{556}) and Fe^{3+} concentration in the range of 20 to 80 μM ($R^2 = 0.9880$) with LOD of 7.12 μM. This nanoprobe realizes the detection of authentic samples successfully, which is expected to serve as a testing kit for analysis in water samples.

Keywords Quantum dots, Carbon dots, Heavy metal ions, Ratiometric fluorescence, Cu^{2+} and Fe^{3+} detection

With the development of modern industry, heavy metal ions pollution in environmental waters has an increasing impact on animals, plants and human health. As two common metal ions, copper ions (Cu^{2+}) and ferric ions (Fe^{3+}) widely exist in nature and play a significant role in life process[1–3]. The formation of intracellular oxidoreductase in the body requires sufficient amounts of copper[4]. However, excessive Cu^{2+} intake has been linked to several physical disorders, including Wilson's disease and Alzheimer's disease[5,6]. The irreversible liver and kidney damage may be caused by long-term accumulation of copper[7]. Unfortunately, due to widespread use of Cu^{2+} in industrial production and daily life, which has been enrolled in the EPA's pollutant list of toxic metal species[8]. Fe^{3+} plays critical roles in cellular metabolism, electron transfer, enzyme catalysis, oxygen hemoglobin production[9]. Both of its deficiency or excess can cause Huntington[10] or Parkinson's disease[11]. Therefore, analysis of heavy metal ions, especially Cu^{2+} and Fe^{3+}, is of great significance for environmental protection and clinical research.

Different analytical methods have been proposed for heavy metal ions detection, including atomic absorption spectrometry[12], electrochemical analysis[13], inductively coupled plasma mass spectroscopy[14], colorimetry[15] and fluorometry[16,17]. Among those ways, fluorescent probes show benefits of simplicity, high sensitivity, low cost and background signals[18,19]. Traditional fluorescence methods are based on intensity of individual emission peak to quantitatively analyze ions, which is susceptible to environmental interferences and results in inaccurate detection[20–22]. To ensure the accurate detection, ratiometric fluorescence probes have self-calibration capabilities. Two emission bands can act as internal reference, removing a majority of interfering factors, including probe concentration, environmental conditions photobleaching and instrumental efficiency[23,24]. However, the largest number of ratiometric fluorescent probes usually focus on detecting a single heavy metal ion specifically. The increased and complex detection requirements of multiple heavy metal ions are urgently needed.

Among fluorescent probes, various fluorescent nanomaterials attract extensive interest, such as metal nanoclusters, quantum dots (QDs) and carbon dots (CDs), etc[25]. The CDs are new carbon-based nanomaterials, the size of which less than 10 nm with spherical particles[26]. Compared with QDs, CDs have better performance, including low toxicity, low cost, simple synthesis, photo stability, adjustable optical properties, good

Institute of Food & Nutrition Science and Technology, Shandong Academy of Agricultural Sciences, Jinan 250100, China. ✉email: chunlei_y@163.com; nkzhhw@163.com

biocompatibility and water solubility[27]. Herein, we innovatively developed a N-doped carbon dots (N-CDs)-based ratiometric fluorescent nanoprobe (N-CDs/OPD) for detection of Cu^{2+} and Fe^{3+} in aqueous solution (Fig. 1). The N-CDs were synthesized via one-step solvothermal treatment of methionine and formamide. Due to inter filter effect (IFE) between metal ion and carbon dots, the N-CDs exhibited a Cu^{2+} and Fe^{3+} fluorescence quenching response properties. After Cu^{2+} and Fe^{3+} mixed with this probe, the fluorescence of N-CDs (436 nm) was quenched and a new peak at 556 nm (DAP) appeared. Cu^{2+}/Fe^{3+} would quench CDs' fluorescence and oxidize o-phenylenediamine (OPD) to 2,3-diaminophenazine (DAP). This strategy realized the fluorescence ratiometric detection of Cu^{2+} and Fe^{3+} in authentic samples successfully, which broadens the potential application of carbon dots.

Experimental section

Materials and apparatus

o-phenylenediamine (OPD), methionine and formamide and were obtained from Shanghai Aladdin Biochemical Techonology Co., Ltd. Phosphoric acid (H_3PO_4) and acetic acid (HAc) were purchased from Sinopharm Chemical Reagent Co. Cu^{2+} standard solution, Fe^{3+} standard solution, boric acid (H_3BO_3), NaOH, cobalt chloride hexahydrate ($CoCl_2{\cdot}6H_2O$), ferrous sulfate heptahydrate ($FeSO_4{\cdot}7H_2O$), nickel (II) sulfate hexahydrate ($NiSO_4{\cdot}6H_2O$), barium chloride dihydrate ($BaCl_2{\cdot}2H_2O$), chromium (III) nitrate nonahydrate ($Cr(NO_3)_3{\cdot}2H_2O$), KCl, $CaCl_2$, NaCl, $MgCl_2$, $MnCl_2$ and $ZnCl_2$ were acquired from Shanghai Macklin Biochemical Technology Co., Ltd. The section of "apparatus" was in "supplementary information".

Synthesis of N-doped carbon dots

N-doped carbon dots (N-CDs) were synthesized by solvothermal synthesis approach with precursors of methionine and formamide. 0.2093 g of methionine was dissolved in 12.5 mL of formamide with ultrasound for 30 min. This mixed solution was added into a Teflon-lined stainless steel autoclave (50 mL) for 1 h with 180 °C. After the system cooling to room temperature, the light brown supernatant was filtered by filter membrane of 0.22 μm to remove large particles. Then, the solution was purified with dialysis bag (molecular weight cut-off of 1000 Da) for 8 h. And finally, the purified product stored in a refrigerator at 4 °C for further use.

Fluorescent detection of Cu2+ and Fe3+

The stock solution concentrations of Cu^{2+} and Fe^{3+} standard solution was 10 mM, respectively. 150 μL of Britton-Robinson buffer [pH 5.3(Cu^{2+}) 5.8(Fe^{3+}), 40 mM], ultrapure water, 150 μL of o-phenylenediamine solution (1 mM), various concentrations of Cu^{2+}/Fe^{3+} solution were blended and diluted to 1.4 mL. After 60 min/10 min still standing at room temperature, 100 μL of N-doped carbon dots was added to above system. Fluorescence measurements were carried out under the excitation wavelength at 360 nm. It was used as the ordinate that the ratio of fluorescence intensity at 436 nm and 556 nm wavelengths (F_{436}/F_{556}). Concentrations of Cu^{2+}/Fe^{3+} were regarded as horizontal ordinate and drawing standard curve for Cu^{2+} and Fe^{3+} detection.

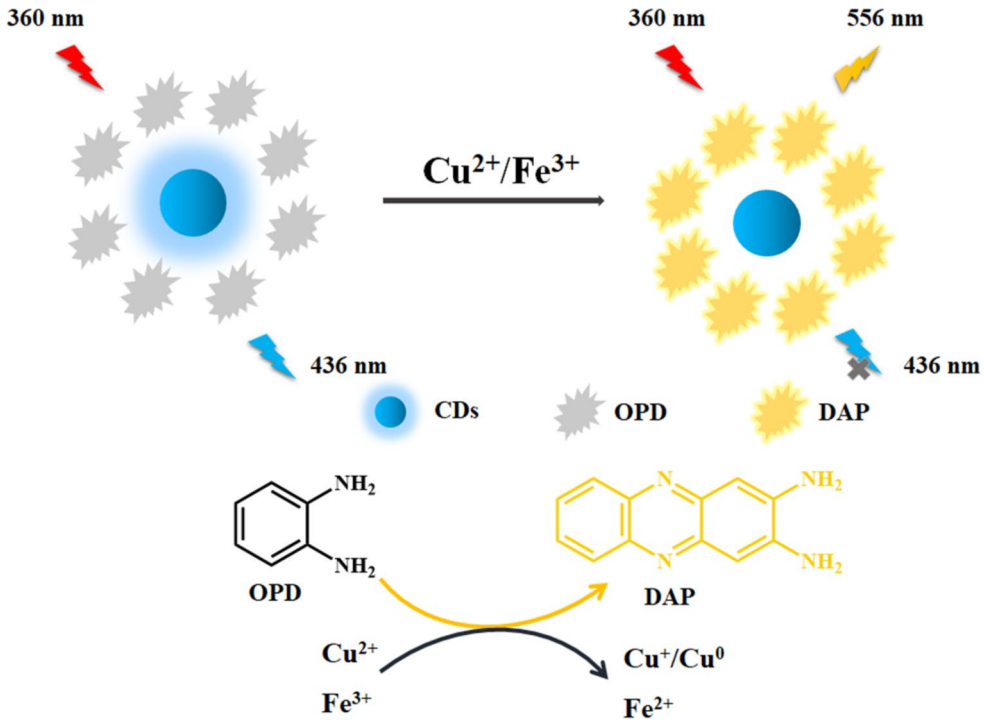

Fig. 1. Schematic illustration of ratiometric fluorescent nanoprobe (N-CDs/OPD) for Cu^{2+} and Fe^{3+} detection.

In order to realize the Cu^{2+} and Fe^{3+} detection in tap water, samples were spiked with various concentrations of Cu^{2+} (20 μM, 30 μM) and Fe^{3+} (40 μM, 60 μM). After that, the samples were measured by this probe using the same experimental procedures as above. These fluorescent spectra were measured and concentrations of spiked samples were calculated by corresponding standard curve.

Selectivity of the proposed nanoprobe

150 μL of Britton-Robison buffer (pH 5.3, 40 mM), 150 μL of o-phenylenediamine solution (1 mM), the same concentration of Cu^{2+}/Fe^{3+} standard solution, or pure water sample as blank sample, various metal interference ions (K^+, Na^+, Ca^{2+}, Mg^{2+}, Ba^{2+}, Zn^{2+}, Co^{2+}, Mn^{2+}, Fe^{2+}, Ni^{2+} and Cr^{3+}) mixed well and diluted to 1.4 mL. 100 μL of N-CDs were added to the above mixture after standing for 60 min. These fluorescent spectra were collected under 360 nm excitation wavelength.

Results and discussion

Characterization and optical properties of N-doped carbon dots

The N-doped carbon dots (N-CDs) were synthesized by solvothermal method with a simple procedure. As depicted in Fig. 2A, the TEM image indicates N-CDs have a monodisperse spherical structure with average diameter of 2 nm. In order to certify element components of N-CDs, XPS measurement was performed. The XPS full spectrum of N-CDs reflects five characteristic peaks, which represent C 1s, N 1s, O 1s, S 2s and S 2p, respectively (Fig. 2B). Atomic percentages of C, N, O and S were 52.23%, 8.06%, 31.01% and 8.71% by calculation, which showing the major components of N-CDs and doped by S and N. The high-resolution XPS spectra of N-CDs (C 1s, N 1s, O 1s and S 2p) are displayed in Fig. 2C–F. As shown in Fig. 2C, the high-resolution XPS spectrum of C 1s was deconvolved into two characteristic peaks, which were attributed to C = O (288.5 eV) and C-O/C = C (285.6 eV) bonds. High-resolution spectra of N 1s (Fig. 2D) displayed three kinds of N: pyrrole N (401.1 eV), amino N (400.3 eV) and pyridine N (399.3 eV)[28,29]. The high-resolution XPS spectra of O 1s (Fig. 2E) locates peaks at 532.1 eV and 533.0 eV, which associate with C-O and C = O bonds. As demonstrated in Fig. 1F, the S 2p spectrum illustrates two major peaks of 164.8 eV and 163.7 eV, which correspond to S 2p1/2 and S 2p3/2 bonding[30].

The FT-IR spectrum also shows the surface functional groups of N-CDs (Fig. 3A). A broad absorption bands at 3200–3600 cm^{-1} is attributed to stretching vibrations of O–H/N–H[31]. The peak located around 2876 cm^{-1} and 1301 cm^{-1} are regarded as stretching vibration of C–H[32,33]. Moreover, these specific peaks located at 1049 cm^{-1}, 1387 cm^{-1}, 1602 cm^{-1} and 1665 cm^{-1} represent the stretching vibration of C–O, C–N, C = C and C = O groups, respectively[29,34–36]. These results demonstrate the surface of carbon dots is decorated by oxygen containing and amino groups, and CDs doping with N are in accordance with FT-IR data. As demonstrated in Fig. 3B, these fluorescence emission spectra of N-CDs with different excitation wavelengths were measured. The emission peaks of N-CDs exhibit a slight red shift from 388 nm to 444 nm with the excitation wavelength from 310 to 370 nm, indicating the excitation-dependent emission of N-CDs. The property of excitation-dependence can be caused by surface heterogeneity of functional groups[37].

When N-CDs were excited at 360 nm, a maximum fluorescence emission intensity was acquired at 436 nm (Fig. 3C). As depicted in inset photograph of Fig. 3C, the as-prepared N-CDs appear pale brown color under daylight and emit bright blue fluorescence with 365 nm UV light. The N-CDs may be acted as a fluorescence

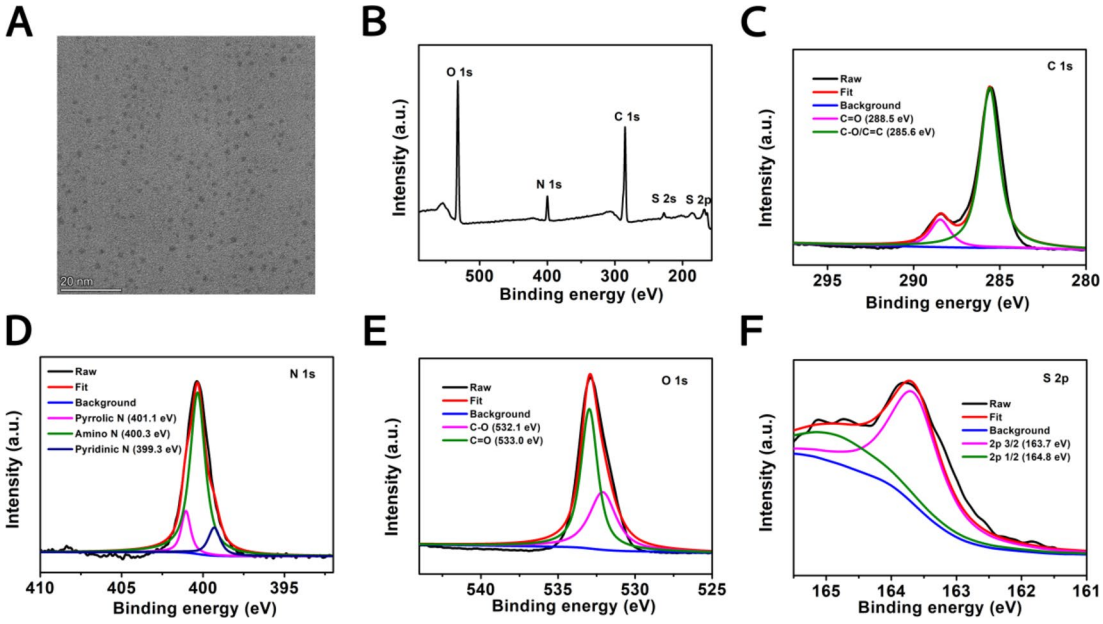

Fig. 2. (**A**) TEM image of N-CDs, (**B**) XPS analysis of N-CDs, (**C–F**) High-resolution XPS spectra of C 1s, N 1s, O 1s and S 2p of N-CDs.

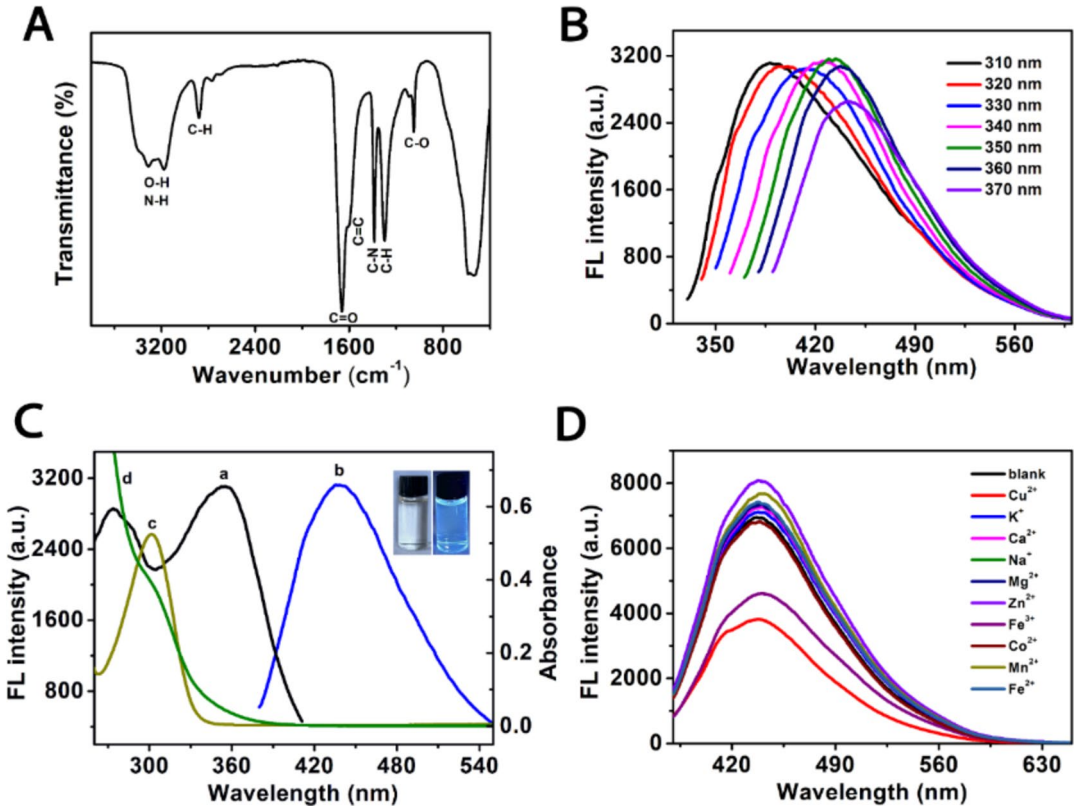

Fig. 3. (**A**) FT-IR spectrum of N-CDs, (**B**) Fluorescence emission spectra of N-CDs with different excitation wavelengths in range of 310 nm to 370 nm. (**C**) Fluorescence excitation (a) and emission (b) spectra of N-CDs, UV-vis spectra of Cu^{2+}(c) and Fe^{3+}(d). (**D**) Fluorescence emission spectra of N-CDs mixed with different metal ions (from top to bottom: Zn^{2+}, Mn^{2+}, Fe^{2+}, Mg^{2+}, Na^{+}, Ca^{2+}, K^{+}, blank, Co^{2+}, Fe^{3+}, Cu^{2+}).

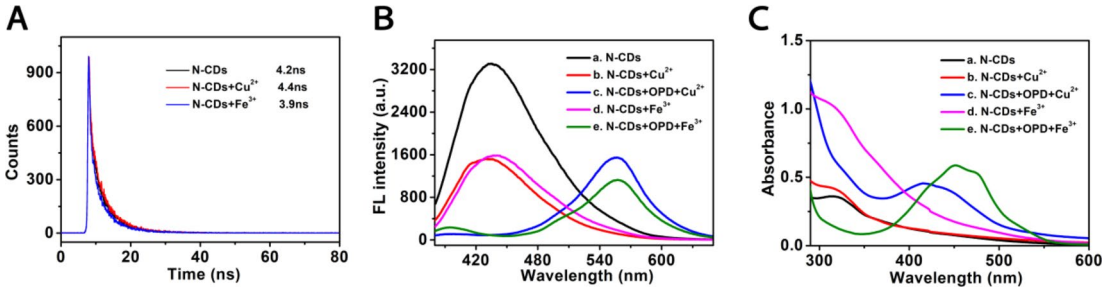

Fig. 4. (**A**) Fluorescence lifetime curves of N-CDs in absence and presence of Cu^{2+} and Fe^{3+}. (**B**) Fluorescence spectra of a: N-CDs, b: N-CDs + Cu^{2+}, c: N-CDs + OPD + Cu^{2+}, d: N-CDs + Fe^{3+}, e: N-CDs + OPD + Fe^{3+}. (**C**) UV–Vis absorption spectra of a: N-CDs, b: N-CDs + Cu^{2+}, c: N-CDs + OPD + Cu^{2+}, d: N-CDs + Fe^{3+}, e: N-CDs + OPD + Fe^{3+}.

probe for Cu^{2+} and Fe^{3+} detection due to their optical property. To examine the selectivity of N-CDs for Cu^{2+} and Fe^{3+}, different interfering metal ions were measured with N-CDs (Fig. 3D). The fluorescent intensity of N-CDs with relevant metal ions had little changes, while fluorescence quenching occurred with Cu^{2+} and Fe^{3+}. These comparison data of fluorescence spectra demonstrate the excellent specificity of N-CDs.

Feasibility analysis and condition optimization

To testify the feasibility of this probe, the sensing mechanism need to be studied. The as-prepared N-CDs can be exploited as a probe to detect cupric ion and ferric ion. We speculated that the fluorescence quenching mechanism of N-CDs was static quenching, which can be strongly determined by fluorescence lifetime measurement. Static quenching usually does not change the fluorescence lifetime[38]. As demonstrated in Fig. 4A, compared with lifetime of N-CDs in the presence of Cu^{2+} and Fe^{3+}, the three lifetime curves almost overlap, which illustrates the static quenching effect. In addition, the absorption peak of Cu^{2+} and Fe^{3+} (Fig. 3C) and excitation peak of N-CDs

overlap significantly. Based on the almost unaffected lifetime curve of N-CDs by metal ion, it is certified that the existence of inter filter effect (IFE) between metal ion and carbon dots.

To realize the ratiometric fluorescent detection of Cu^{2+} and Fe^{3+}, we investigated the response mechanisms by the UV-vis absorption and fluorescence spectra. As shown in Fig. 4B, after Cu^{2+} and Fe^{3+} mixed with N-CDs/OPD system, the fluorescence of N-CDs (436 nm) was quenched and a new peak at 556 nm (DAP) appeared. Because Cu^{2+}/Fe^{3+} would quench the fluorescence of N-CDs and oxidize OPD to DAP. In Fig. 4C, N-CDs exhibits an obvious UV-vis absorption peak at 319 nm. The N-CDs/OPD appeared new broad absorption peaks attributed to DAP in the presence of Cu^{2+} and Fe^{3+}, which overlaps significantly with the excitation spectrum of N-CDs. These phenomena may be relative to Cu^{2+}/Fe^{3+} react with OPD, causing the generation of new substance. These results can explain the further fluorescence quenching occurs for N-CDs induced by Cu^{2+} and Fe^{3+} after the addition of OPD in Fig. 4B. In terms of theoretical mechanisms, Cu^{2+} and Fe^{3+} both have a strong oxidation in acidic conditions, which could oxidize OPD to DAP in this sensing system. The relevant reaction process is shown in Fig. 1. Cu^{2+} oxidized OPD to DAP and it was reduced to Cu^{+}/ Cu^{0}. Fe^{3+} oxidized OPD to DAP and it was reduced to Fe^{2+}.

Optimized experimental conditions (pH values, concentration of OPD and reaction time) were employed to obtain optimal response for Cu^{2+} and Fe^{3+} detection. As illustrated in Fig. 5A and C, as pH values increase, F_{436}/F_{556} (the fluorescent peak of N-CDs at 436 nm and DAP at 556 nm) reduces and attains a stable condition. Therefore, pH 5.3 and pH 5.8 are selected as proper pH values for Cu^{2+} and Fe^{3+} detection respectively. To investigate whether pH has an effect on the fluorescence of N-CDs, the fluorescence response of N-CDs under different time with pH 7.0 and pH 5.3 were measured (Fig. S1). The N-CDs have an excellent fluorescent stability in weak acidic and neutral environment. Meanwhile, the OPD concentrations of Cu^{2+} and Fe^{3+} measurement have similar change trend (Figs. S2, S3). Thus, 100 μM of OPD was chosen for next test. Furthermore, the reaction time of Cu^{2+} and Fe^{3+} are shown in Fig. 5B and D. These values of F_{436}/F_{556} for Cu^{2+} and Fe^{3+} remain steady after 60 min and 10 min, respectively. Hence, 60 min and 10 min are selected as optimal reaction time for Cu^{2+} and Fe^{3+} detection.

Fluorescent ratiometric detection of copper ions and ferric ions

The analytical performance of this probe for Cu^{2+} and Fe^{3+} was evaluated under optimized experimental conditions. As depicted in Fig. 6A, keeping the concentrations of N-CDs and OPD constant, the fluorescence

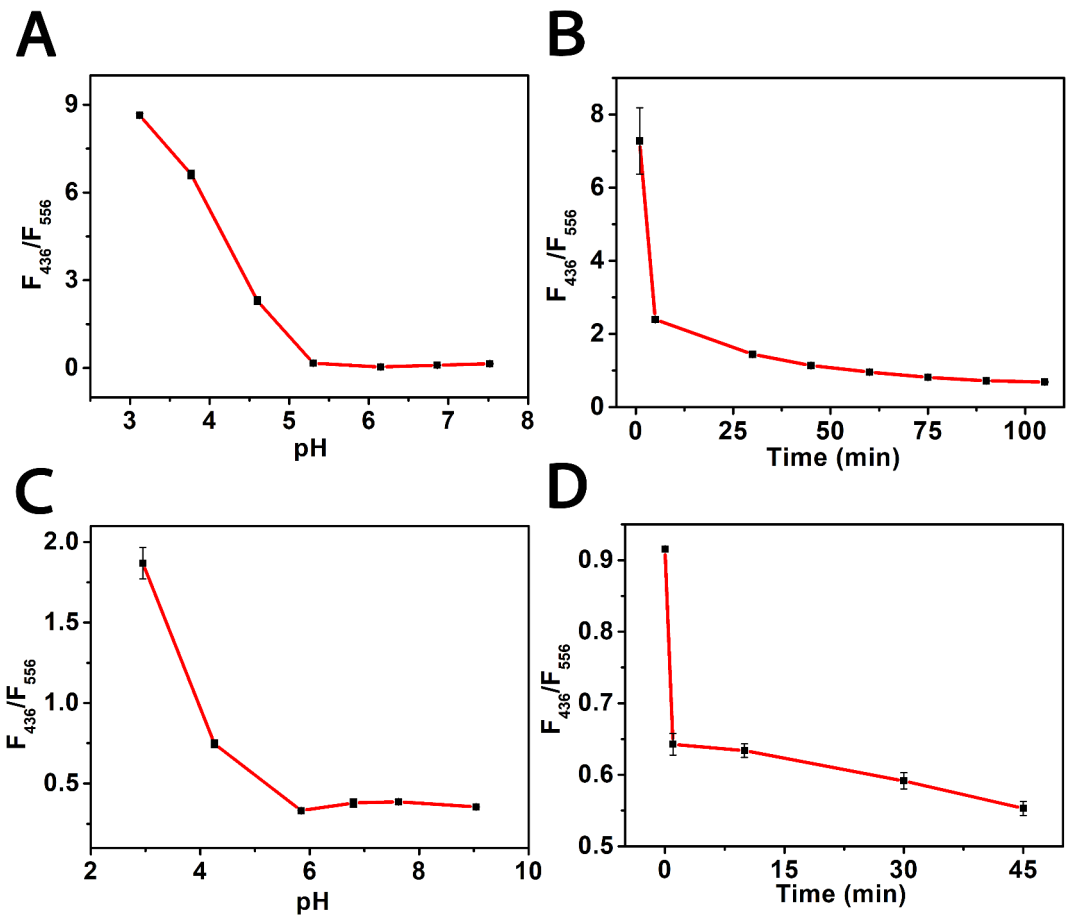

Fig. 5. The effect of (**A**) pH values and (**B**) reaction time with Cu^{2+} detection. The effect of (**C**) pH values and (**D**) reaction time with Fe^{3+} detection.

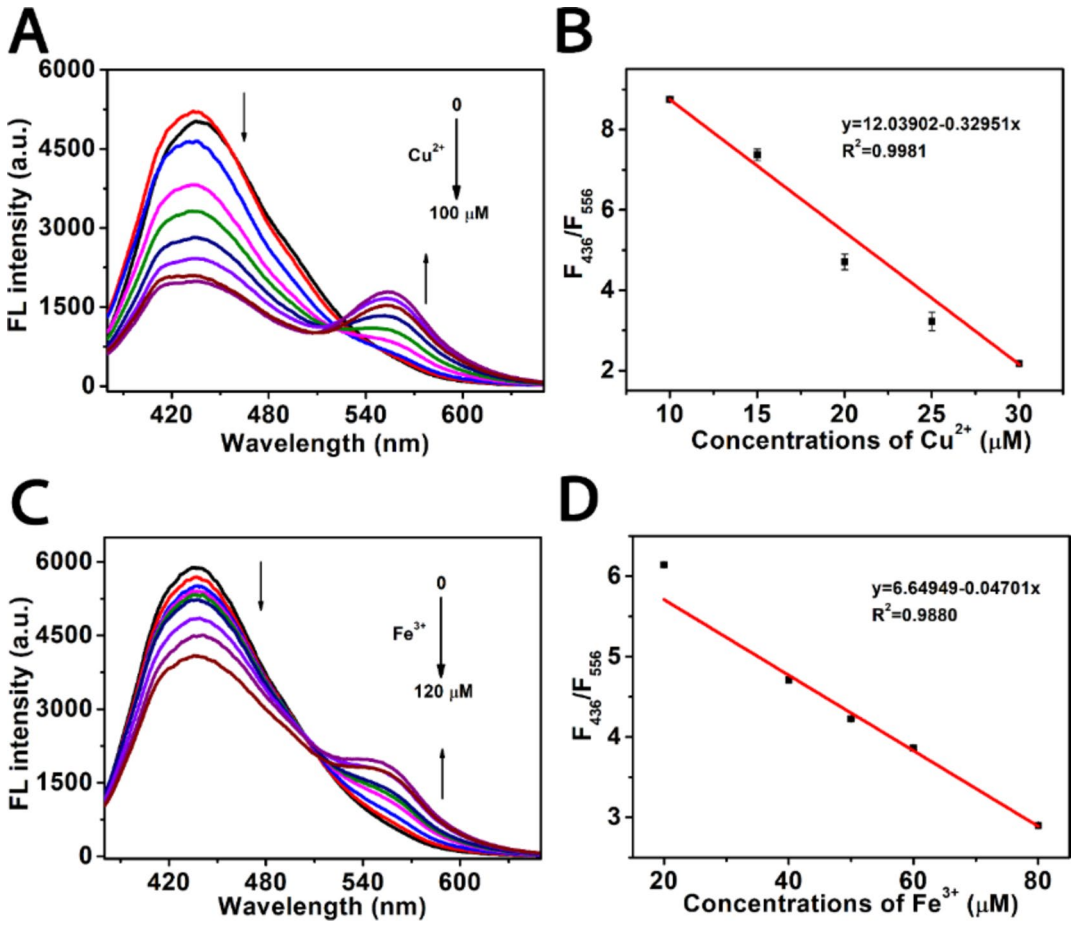

Fig. 6. (**A**) Changes in fluorescence intensity of nanoprobe (N-CDs/OPD) in different concentrations (0, 10, 15, 20, 25, 30, 40, 70 and 100 μM) of Cu^{2+}. (**B**) The linear plot of F_{436}/F_{556} against Cu^{2+} concentration (10, 15, 20, 25 and 30 μM). (**C**) Changes in fluorescence intensity of nanoprobe (N-CDs/OPD) in different concentrations (0, 10, 20, 40, 50, 60, 80, 100 and 120 μM) of Fe^{3+}. (**D**) The linear plot of F_{436}/F_{556} against concentration of Fe^{3+} (20, 40, 50, 60 and 80 μM).

emission peak at 436 nm (N-CDs) reduces whereas 556 nm (DAP) increases with enhancive amount of Cu^{2+} (0–100 μM). The dependence of Cu^{2+} concentration and fluorescence ratio (F_{436}/F_{556}) is shown in Fig. S4. When the Cu^{2+}concentration enhanced, F_{436}/F_{556} declined and achieved equilibrium. As displayed in Fig. 6B, the nice linear correlation is obtained between F_{436}/F_{556} and Cu^{2+} concentration in range of 10 to 30 μM with $R^2 = 0.9981$. The limit of detection (LOD) was determined by 3Sd/K, where Sd represents standard deviation of blank samples and K represents slope of calibration line. The limit detection of Cu^{2+} was calculated to be 0.86 μM. Similarly, as shown in Fig. 6C, the fluorescent ratiometric response of this probe for Fe^{3+} shows same variation trend with rising Fe^{3+} concentrations (0–120 μM) with optimal experimental conditions. A steady reduction in fluorescence ratio is recorded with Fe^{3+} concentration increasing (Fig. S5). In Fig. 6D, a good linear relationship ($R^2 = 0.9880$) is obtained between fluorescence ratio (F_{436}/F_{556}) and Fe^{3+} concentration in range of 20 to 80 μM with LOD = 7.12 μM.

In Fig. 7, to access the selectivity of Cu^{2+} and Fe^{3+} detection, we performed fluorescent response of N-CDs/OPD toward various potentially metal ions, including K^+, Na^+, Ca^{2+}, Mg^{2+}, Ba^{2+}, Zn^{2+}, Co^{2+}, Mn^{2+}, Fe^{2+}, Ni^{2+} and Cr^{3+}. Figure 6 shows that only Cu^{2+} and Fe^{3+} could lead to significant increase of fluorescence intensity ratio and the influence of other metal ions is negligible. To examine the precision and accuracy of this nanoprobe, tap water samples were spiked with Cu^{2+} and Fe^{3+} ions and analyzed with this method in triple replicates with same conditions. These relative standard deviations (RSD) and recoveries results for the spiked samples are listed in Table 1. These results indicate a good consistency between added and found concentrations of Cu^{2+} and Fe^{3+}. These recoveries in tab water samples are between 98.2% and 109.3%, and the RSD values are less than 1.40%. In order to strengthen scientific significance of this probe, standard addition detection of Cu^{2+} and Fe^{3+} in domestic wastewater were performed in Table S1, which acquired relatively good results. Therefore, these results demonstrate the probe has a good accuracy and precision for the analysis of tracking Fe^{3+} and Cu^{2+} in real water. Compared with other analytical methods in Table S2, the detection performance of current method was superior or comparable to previously reported probes for Cu^{2+} and Fe^{3+} detection. The above results indicate that the simple and sensitive fluorescent ratiometric system has potential for monitoring the level of copper ions and ferric ions in water.

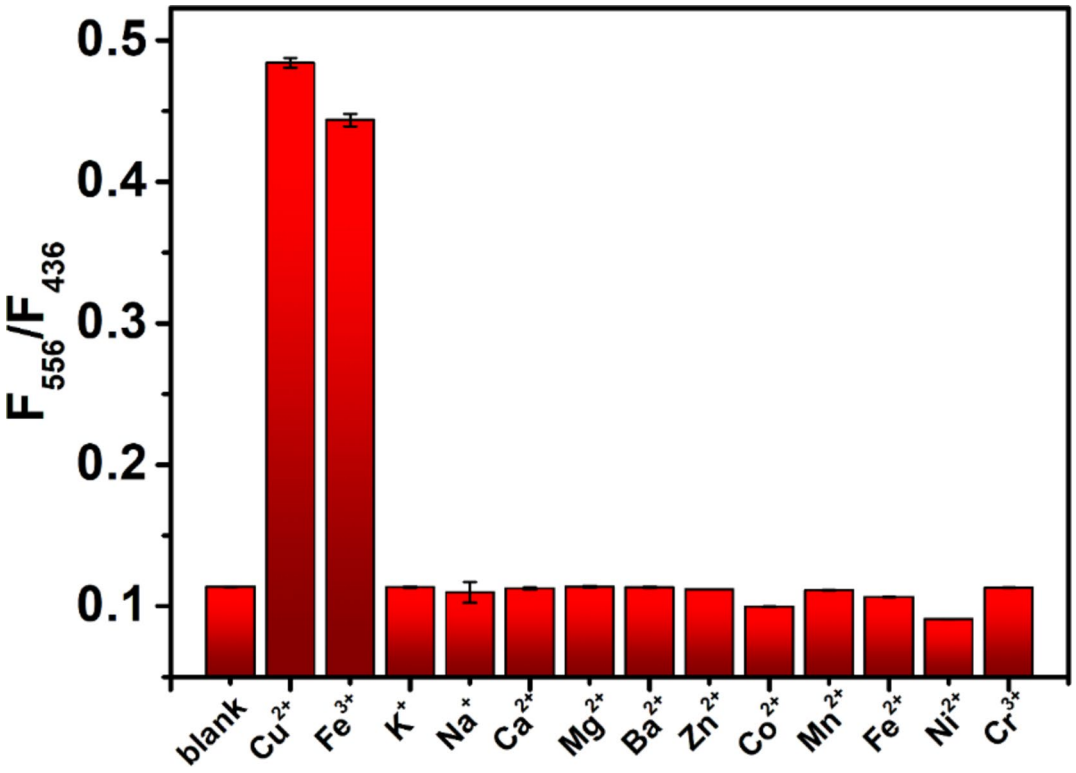

Fig. 7. Fluorescent intensity ratio of N-CDs/OPD in presence of different metal ions for Cu^{2+} and Fe^{3+} detection (interfering and target ions from left to right: blank, Cu^{2+}, Fe^{3+}, K^{+}, Na^{+}, Ca^{2+}, Mg^{2+}, Ba^{2+}, Zn^{2+}, Co^{2+}, Mn^{2+}, Fe^{2+}, Ni^{2+} and Cr^{3+}, concentrations: 100 μM).

Samples	Spiked (μM)	Found (μM)	Recovery (%), $n=3$	RSD (%), $n=3$
Cu^{2+}	20.00	21.86 ± 0.16	109.3	0.71
	30.00	29.46 ± 0.27	98.2	0.88
Fe^{3+}	40.00	41.95 ± 0.61	104.9	1.40
	60.00	59.36 ± 0.61	98.9	0.92

Table 1. Results of the standard addition detection of Cu^{2+} and Fe^{3+} in tap water.

Conclusion

In conclusion, a cost-effective N-doped carbon dots-based ratiometric fluorescent nanoprobe (N-CDs/OPD) is designed for the detection of copper ions and ferric ions. The OPD could be oxidized to DAP by Cu^{2+} and Fe^{3+}. The N-CDs have fluorescence quenching response characteristics of Cu^{2+} and Fe^{3+} because of inner filter effect. After addition of Cu^{2+} and Fe^{3+}, the fluorescence of N-CDs (436 nm) is quenched and a new peak at 556 nm (DAP) appears, which realizes fluorescence ratiometric change. Therefore, this strategy enables the fluorescence ratiometric determination of Cu^{2+} and Fe^{3+} in authentic samples successfully, which has potential application for point-of-care testing.

Data availability

The datasets used and analysed during the current study available from the corresponding author, Y.C. on reasonable request.

Received: 25 December 2024; Accepted: 4 February 2025
Published online: 20 February 2025

References

1. Liu, W. et al. Efficient and selective sensing of Cu^{2+} and UO_2^{2+} by a europium metal-organic framework. *Talanta* **196**, 515–522. https://doi.org/10.1016/j.talanta.2018.12.088 (2019).
2. Mi, X. et al. Tunable light emission and multiresponsive luminescent sensitivities in aqueous solutions of two series of lanthanide metal-organic frameworks based on structurally related ligands. *ACS Appl. Mater. Interface*. **11**, 7914–7926. https://doi.org/10.1021/acsami.8b18320 (2019).

3. Yu, Y. E. et al. Multiresponsive luminescent sensitivities of a 3D Cd-CP with visual turn-on and ratiometric sensing toward Al^{3+} and Cr^{3+} as well as turn-off sensing toward Fe^{3+}. *Inorg. Chem.* **59**, 3828–3837. https://doi.org/10.1021/acs.inorgchem.9b03496 (2020).
4. Sakaguchi, T., Okunaga, R., Irie, S., Urushisaki, M. & Hashimoto, T. Carbon dioxide-permselective polymer membranes composed of poly(vinyl ether)-based, ABA-type triblock copolymers with pendant oxyethylene chains. *Polym. Bull.* **74**, 2017–2031. https://doi.org/10.1007/s00289-016-1820-2 (2017).
5. Patel, R. & Aschner, M. Commonalities between copper neurotoxicity and Alzheimer's disease. *Toxics* **9**, 1 (2021).
6. Russell, K., Gillanders, L. K., Orr, D. W. & Plank, L. D. Dietary copper restriction in Wilson's disease. *Eur. J. Clin. Nutr.* **72**, 326–331. https://doi.org/10.1038/s41430-017-0002-0 (2018).
7. Bost, M. et al. Dietary copper and human health: current evidence and unresolved issues. *J. Trace Elem. Med. Biol.* **35**, 107–115. https://doi.org/10.1016/j.jtemb.2016.02.006 (2016).
8. Kleyer, H., Tecon, R. & Or, D. Resolving species level changes in a representative soil bacterial community using microfluidic quantitative PCR. *Front. Microbiol.* **8**, 17. https://doi.org/10.3389/fmicb.2017.02017 (2017).
9. Li, S. et al. A novel solvent-dependently bifunctional NIR absorptive and fluorescent ratiometric probe for detecting Fe^{3+}/Cu^{2+} and its application in bioimaging. *Sens. Actuators B Chem.* **224**, 661–667. https://doi.org/10.1016/j.snb.2015.10.086 (2016).
10. Crabtree, R. H. Principles of bioinorganic chemistry. *Science* **266**, 1591 (1994).
11. Burdo, J. R. & Connor, J. R. Brain iron uptake and homeostatic mechanisms: An overview. *BioMetals* **16**, 63–75. https://doi.org/10.1023/A:1020718718550 (2003).
12. Pourjavid, M. R., Arabieh, M., Yousefi, S. R. & Akbari Sehat, A. Interference free and fast determination of manganese(II), iron(III) and copper(II) ions in different real samples by flame atomic absorption spectroscopy after column graphene oxide-based solid phase extraction. *Microchem J.* **129**, 259–267. https://doi.org/10.1016/j.microc.2016.07.008 (2016).
13. Xu, W., Zhu, L., Shao, X., Huang, K. & Luo, Y. An electrochemical biosensor based on nucleic acids enzyme and nanochannels for detecting copper (II) ion. *Biosens. Bioelectron.* **120**, 168–174. https://doi.org/10.1016/j.bios.2018.08.033 (2018).
14. Arslan, Z., Oymak, T. & White, J. Triethylamine-assisted $mg(OH)_2$ coprecipitation/preconcentration for determination of trace metals and rare earth elements in seawater by inductively coupled plasma mass spectrometry (ICP-MS). *Anal. Chim. Acta.* **1008**, 18–28. https://doi.org/10.1016/j.aca.2018.01.017 (2018).
15. Zhang, Y., Ren, T., Tian, H., Jin, B. & He, J. Hydrogel-encapsulated enzyme facilitates colorimetric acute toxicity assessment of heavy metal ions. *ACS Appl. Mater. Interface.* **10**, 26705–26712. https://doi.org/10.1021/acsami.8b08949 (2018).
16. Geng, R. et al. Bimetallic Ag/Zn-ZIF-8: an efficient and sensitive probe for Fe^{3+} and Cu^{2+} detection. *Colloids Surf. Physicochem Eng. Aspects.* **632**. https://doi.org/10.1016/j.colsurfa.2021.127755 (2022).
17. Kaushik, R. et al. Multianalytes sensing probe: fluorescent moisture detection, smartphone assisted colorimetric phosgene recognition and colorimetric discrimination of Cu^{2+} and Fe^{3+} ions. *Sens. Actuators B Chem.* **328**. https://doi.org/10.1016/j.snb.2020.129026 (2021).
18. Mahata, P., Mondal, S. K., Singha, D. K. & Majee, P. Luminescent rare-earth-based MOFs as optical sensors. *Dalton Trans.* **46**, 301–328. https://doi.org/10.1039/C6DT03419E (2017).
19. Zhao, S. N., Wang, G., Poelman, D. & Voort, P. V. Luminescent lanthanide MOFs: a unique platform for chemical sensing. *Materials* **11**, 1 (2018).
20. Li, N. N. et al. A novel dimer-induced AIE material as a nano-sensor for colormetric and ratiometric sensing of Erythromycin and metal ions (Zn^{2+}, Cd^{2+} and Cu^{2+}) with different dissociation and re-aggregation processes and cellular imaging applications. *Dyes Pigm.* **184**, 108872. https://doi.org/10.1016/j.dyepig.2020.108872 (2021).
21. Bhati, A. et al. Self-doped nontoxic red-emitting Mg–N-embedded carbon dots for imaging, Cu(ii) sensing and fluorescent ink. *New. J. Chem.* **42**, 19548–19556. https://doi.org/10.1039/C8NJ04754E (2018).
22. Wang, C., Bi, X., Wang, M., Zhao, X. & Lin, Y. Dual-channel online optical detection platform integrated with a visible light absorption approach for continuous and simultaneous in vivo monitoring of ascorbic acid and copper(II) ions in a living rat brain. *Anal. Chem.* **91**, 16010–16016. https://doi.org/10.1021/acs.analchem.9b04783 (2019).
23. Chuong, T. T. et al. Dual-reporter SERS-based biomolecular assay with reduced false-positive signals. *PNAS* **114**, 9056–9061. https://doi.org/10.1073/pnas.1700317114 (2017).
24. Qiu, Z., Shu, J., Liu, J. & Tang, D. Dual-channel photoelectrochemical ratiometric aptasensor with up-converting nanocrystals using spatial-resolved technique on homemade 3D printed device. *Anal. Chem.* **91**, 1260–1268. https://doi.org/10.1021/acs.analchem.8b05455 (2019).
25. Wang, Y. F. et al. One-pot synthesis of boron and nitrogen co-doped silicon-carbon dots for fluorescence enhancement and on-site colorimetric detection of dopamine with high selectivity. *Appl. Surf. Sci.* **573**, 151457. https://doi.org/10.1016/j.apsusc.2021.151457 (2022).
26. Li, D. et al. Supra-(carbon nanodots) with a strong visible to near-infrared absorption band and efficient photothermal conversion. *Light Sci. Appl.* **5**, e16120. https://doi.org/10.1038/lsa.2016.120 (2016).
27. Yue, J. et al. One-step synthesis of acriflavine-based carbon dots for adenine detection and a theoretical study on the detection mechanism. *Microchem J.* **148**, 73–78. https://doi.org/10.1016/j.microc.2019.04.041 (2019).
28. Wang, X. et al. Bridging environmental and biological monitoring: constructing platform for hexavalent chromium detection and cancer-cells screening based on red fluorescent carbonized polymer dots. *Chem. Eng. J.* **451**, 138524. https://doi.org/10.1016/j.cej.2022.138524 (2023).
29. Qin, J. et al. Carbon nanodot-based humidity sensor for self-powered respiratory monitoring. *Nano Energy*. **101**, 107549. https://doi.org/10.1016/j.nanoen.2022.107549 (2022).
30. Wang, L. et al. Mesoporous nitrogen, sulfur co-doped carbon dots/CoS hybrid as an efficient electrocatalyst for hydrogen evolution. *J. Mater. Chem. A*. **5**, 2717–2723. https://doi.org/10.1039/C6TA09580A (2017).
31. Tang, M., Ren, G. & Chai, F. A facile synthesis of magnetic fluorescence Fe_3O_4-carbon dots for the detection and removal of Hg^{2+}. *New. J. Chem.* **44**, 6635–6642. https://doi.org/10.1039/D0NJ00275E (2020).
32. Mondal, S., Vinod, C. P. & Gautam, U. K. Autophagy' and unique aerial oxygen harvesting properties exhibited by highly photocatalytic carbon quantum dots. *Carbon* **181**, 16–27. https://doi.org/10.1016/j.carbon.2021.04.054 (2021).
33. Tao, Y., Ju, E., Ren, J. & Qu, X. Polypyrrole nanoparticles as promising enzyme mimics for sensitive hydrogen peroxide detection. *Chem. Commun.* **50**, 3030–3032. https://doi.org/10.1039/C4CC00328D (2014).
34. Yan, F. et al. Color emission carbon dots with quench-resixastant solid-state fluorescence for light-emitting diodes. *ACS Sustain. Chem. Eng.* **9**, 3901–3908. https://doi.org/10.1021/acssuschemeng.0c09133 (2021).
35. Wang, J. et al. Tunable full-color solid-state fluorescent carbon dots for light emitting diodes. *Carbon* **190**, 22–31. https://doi.org/10.1016/j.carbon.2022.01.001 (2022).
36. Tang, X. et al. Nitrogen-doped fluorescence carbon dots as multi-mechanism detection for iodide and curcumin in biological and food samples. *Bioact Mater.* **6**, 1541–1554. https://doi.org/10.1016/j.bioactmat.2020.11.006 (2021).
37. Tang, X. et al. Exploration of nitrogen-doped grape peels carbon dots for baicalin detection. *Mater. Today Phys.* **22**. https://doi.org/10.1016/j.mtphys.2021.100576 (2022).
38. Sun, P. et al. The fabrication of N-doped carbon dots by methionine and their utility in sensing Cu^{2+} in real water. *Anal. Methods.* **15**, 1631–1638. https://doi.org/10.1039/D3AY00056G (2023).

Acknowledgements
This research was financially supported by Natural Science Foundation of Shandong Province (No. ZR2023QC284), Agricultural Science and Technology Innovation Project of Shandong Academy of Agricultural Sciences (No. CXGC2024F09).

Author contributions
Yang Chunlei: Conceptualization, Methodology, Formal analysis, Investigation, Writing - Original Draft, Funding acquisition. Xu Guiju: Validation, Writing - Review & Editing. Hou Chenghao: Supervision. Zhang Hongwei: Project administration.

Declarations

Competing interests
The authors declare no competing interests.

Additional information
Supplementary Information The online version contains supplementary material available at https://doi.org/10.1038/s41598-025-89327-z.

Correspondence and requests for materials should be addressed to C.Y. or H.Z.